

---

# Theory and Principles of Operation of Nanophotonic Functional Devices

S. Sangu, K. Kobayashi, A. Shojiguchi, T. Kawazoe, and M. Ohtsu

## 1 Introduction

### 1.1 Nanophotonics for Functional Devices

In response of the need for increased and faster information processing in the near future, miniaturization of optical devices has progressed [1] to the point that it has now almost reached the critical limit determined by the diffraction of conventional propagating light [2, 3]. Since 1990s, researchers have anticipated that optical near-field devices may be one of the first important technologies to overcome this limit; many studies have been performed in various fields such as fundamental physics in nanometric space, optical near-field microscopy and spectroscopy, optical measurement, bioimaging, nanofabrication, and nanophotonic device architecture [4]. An optical near field is the characteristic localized electromagnetic field around a nanometric object, and its decay length, which is smaller than the wavelength of incident light, depends on the size of the object. This size dependence means that optical near fields cannot be separated from matter excitation; in nanometric space, the incident electromagnetic field is modified by matter excitation in an object, and the modified field also affects the object itself and another neighboring one before releasing the energy as far-field photons. This nanometric light–matter interaction must describe as a self-consistent field. The goal is to create nanometric functional devices that are free from light diffraction limits, in which such optical near fields act as information carrier and control signals. These devices are termed *nanophotonic devices*. The localization feature of nanophotonic devices seems to resemble electronic devices in which an electric charge always stays within the device, but in a nanophotonic device, the localized field is able to leave an object and release photons in the far field via optical near-field interaction among several nanometric objects [5]. An important component of nanophotonic devices and nanophotonic device operations is dealing with light–matter interaction with a nanometric system, as well as dissipation of matter excitation energy toward the outer field. Since the signal is

eventually detected as far-field light, nanometric light-matter interaction also needs to control the dissipation process. Hence, the inherent operation of a nanophotonic device in nanophotonics differs from conventional optical and electronic devices.

The advantages of nanophotonic devices include not only miniaturization but also possibilities for novel principles of functional operations that are inherent to nanophotonics. As mentioned above, the physics of nanophotonic devices includes typical matter excited states due to optical near-field interaction, coupling between near- and far-field light, and coupling between matter excitation and phonons. Many of these characteristics have not been considered in conventional optics; the structures within nanophotonic devices may differ from those of conventional devices, since basic principles utilized differ and nanophotonic devices can accomplish functions that have not been possible to date. It is important to consider how these devices should be designed, and to learn how nanophotonic devices can coexist with other devices.

In this chapter, our discussion focuses on how to use the features inherent to nanophotonics in functional device operations, what is possible, and how we can realize the possibilities. Section 1.2 explains some characteristic features of nanophotonics and provides a basic outline of nanophotonic devices.

## 1.2 Inherent Features to Nanophotonics

In general, the following features are indispensable to a functional device: preparation of appropriate input states, propagation of a signal, and control of the signal. Nanophotonics has characteristic features for all of these, none of which are observed in far-field light. This section explains features inherent to nanophotonics: a locally excited state that cannot be created using far-field light, unidirectional energy transfer, and a dependence on excitation number in which coupling between discrete energy levels and the optical near field plays an important role. These are all key features for nanophotonic device operations.

### Locally Excited States

First, we will explain the difference between matter excitation of nanometric objects using far- and near-field light. Figure 1a illustrates nanometric objects being irradiated by far-field light. Since objects located in an area much smaller than the wavelength of the light are simultaneously excited by a uniform field, it is neither possible to examine the state of matter excitation in each object independently nor does the detected far-field light provide any information about the state of excitement in each object. Optical near-field excitation can be accomplished by setting an optical near-field probe, such as a nanometric metallic aperture, an optical fiber probe, and a single molecule. This allows selective irradiation of individual object, and a locally excited

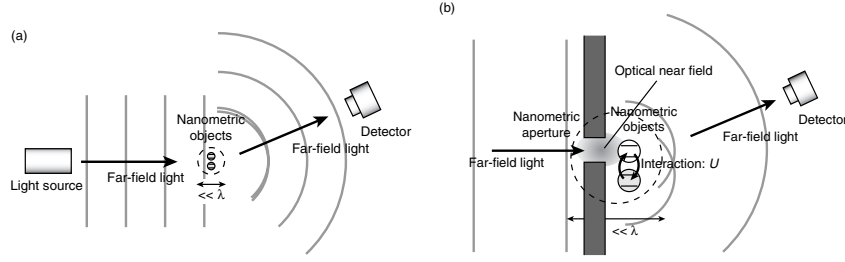


**Fig. 1.** Schematic illustration of nanometric matter excitation by using (a) far-field light and (b) near-field light

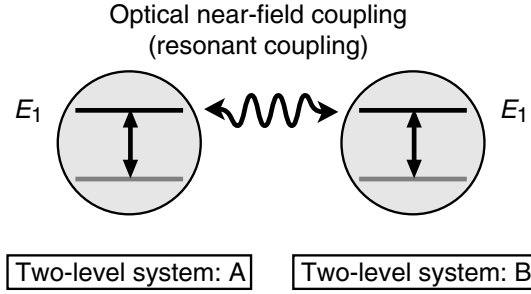


**Fig. 2.** Identical two two-level systems which are coupled via optical near-field interaction

state can be created because of the localized light around the probe. The excited object creates a secondary electromagnetic field that affects neighboring fields via the optical near field, and consistently determining excited states in the system using optical near-field interaction. Figure 1b shows schematics of optical near-field excitation. This asymmetric excitation also influences far-field light which can be detected as an information signal.

The following describes these excited states as algebraic expressions. For simplicity, the discussion is restricted to the coupling of two two-level systems of excitons (see Fig. 2). For far-field excitation, nanometric objects are uniformly excited; a one-exciton state, in which an exciton exists in the system, can thus be written as

$$|1\rangle_s = (|e\rangle_A |g\rangle_B + |g\rangle_A |e\rangle_B) / \sqrt{2}, \quad (1)$$

where  $|e\rangle_i$  and  $|g\rangle_i$  represent exciton state and crystal ground state, respectively. Subscripts,  $i = A$  and  $B$ , label two nanometric objects, and the meaning of subscript  $s$  will be explained later. Equation (1) means that an exciton in an isolated system cannot be distinguished because the exciton exists in both object A and object B with equivalent probabilities.

On the other hand, as mentioned above, an optical near field allows an exciton to be created in an individual object. The exciton prepared in this

system leaves and returns between the two two-level systems for a period depending on the strength of optical near-field coupling, referred to as near-field optical nutation [6,7]. However, if the pumping time is much shorter than the period of near-field optical nutation, locally excited states can be created in this system. Such locally excited states with an exciton in the system can be expressed by a linear combination of coupled states that extends between two objects, as follows:

$$|e\rangle_A |g\rangle_B = (|1\rangle_s + |1\rangle_a)/\sqrt{2}, \quad (2)$$

$$|g\rangle_A |e\rangle_B = (|1\rangle_s - |1\rangle_a)/\sqrt{2}. \quad (3)$$

The right-hand terms in (2) and (3) described states coupled via an optical near field, where the subscripts *s* and *a* refer to symmetric and anti-symmetric states, respectively. It is clear that in the optical near-field excitation, there are two coupled states while far-field light excites only the symmetric state. Note that we did not show the anti-symmetric state in (1), since the state is optically inactive for far-field light. This can be verified using the following relation:  ${}_a\langle 1|\hat{H}_{\text{int}}|g\rangle = 0$ , where  $|g\rangle = |g\rangle_A |g\rangle_B$  and the interaction Hamiltonian refers to (5). Locally excited states are quite important for functional operations in our proposed nanophotonic devices, which are discussed in Sects. 3 and 4.

### Unidirectional Energy Transfer

For functional device operations to manipulate information carriers, an excitation or carrier must transfer unidirectionally from the input to the output terminals. In conventional optical devices, a unidirectional energy transfer can be accomplished by using an optical isolator, which generally uses polarization to block reflected light. Unless polarization is used, the size of optical devices is restricted by light wavelength. In electronic devices, a unidirectional signal transfer is easily attained since electrons flow along an electrical potential. However, as electronic devices become smaller and quantum mechanical effects arise, electrical signals are affected by noise because of universal quantum fluctuations. In a nanophotonic device, signal isolation using light wave characteristics is impossible because of the light diffraction limit, and a signal carrier is composed of electrically neutral quasi-particles of electrons and holes. Thus, a static electrical potential cannot be used to drive them. However, unidirectional exciton energy transfer can be effectively realized using a relaxation process among quantum discrete energy levels [8]. Figure 3 is a schematic image of energy transfer via an optical near field in a system that consists of two nanometric objects with two- and three-energy levels. As mentioned in “Locally Excited States,” optical near-field coupling causes a coherently coupled excited state between the  $E_1$ -level in the two-level system and the  $E_2$ -level in the three-level system, which strengthens when both energies are equal. If excitation can be dropped into the lower  $E_1$ -level in the three-level system before the radiative lifetime of  $E_1$ -level in the two-level system ( $\sim 1$  ns), excitation is confined to the energy level due to off-resonance,

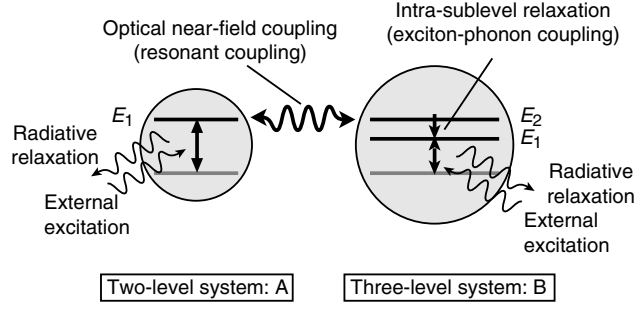


**Fig. 3.** Energy transfer between two-level and three-level systems.  $E_2$ -level in the three-level system is dipole inactive, and thus, the unidirectional energy transfer is achieved only by mediating an optical near field

and irreversibility in the nanometric system is guaranteed except for radiation from the energy level. Section 2 provides a detailed discussion about optical near-field coupling and energy transfer dynamics. In the three-level system, the  $E_2$ -level is generally dipole inactive for far-field light, and thus, unidirectional energy transfer can be achieved by mediating the optical near field.

Since external far- or near-field light can cause excitations in dipole active levels: the  $E_1$ -levels in the two-level and the three-level systems, energy transfer in this system is controllable. A simple switching operation can be constructed using the state-filling nature of excitons excited by the external field. In Sect. 3, a nanophotonic switch that uses energy transfer and state-filling is proposed, and the dynamics of excitation are evaluated both analytically and numerically.

### Dependence of Excitation Number

Although symmetric and anti-symmetric states in (1)–(3) describe one-exciton states, a quite interesting feature is evident in the two-exciton state in the system shown in Fig. 2. The two-exciton state, in which two excitons completely occupy both two-level systems, is algebraically written as

$$|2\rangle_p = |e\rangle_A |e\rangle_B, \quad (4)$$

where number 2 in the left-hand side refers to the two-exciton state. It is valuable to investigate energies for all base states,  $|1\rangle_s$ ,  $|1\rangle_a$ , and  $|2\rangle_p$ . The Hamiltonian for the two-level systems coupled via an optical near-field interaction is given by

$$\hat{H} = \hat{H}_0 + \hat{H}_{\text{int}}, \quad (5)$$

$$\hat{H}_0 = \hbar\Omega\hat{A}^\dagger\hat{A} + \hbar\Omega\hat{B}^\dagger\hat{B}, \quad (6)$$

$$\hat{H}_{\text{int}} = \hbar U(\hat{A}^\dagger\hat{B} + \hat{A}\hat{B}^\dagger), \quad (7)$$

where  $\hat{H}_0$  and  $\hat{H}_{\text{int}}$  represent the unperturbed and interaction Hamiltonian, respectively.  $(\hat{A}^\dagger, \hat{A})$  and  $(\hat{B}^\dagger, \hat{B})$  are the fermionic creation and annihilation

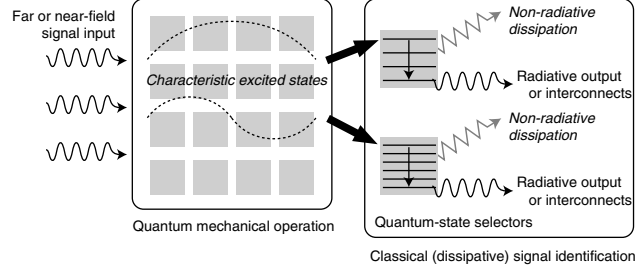


**Fig. 4.** Conceptual structure of nanophotonic devices, which consists of a quantum mechanical part and a classical dissipative part. Quantum mechanical part builds up characteristic excited states and classical dissipative part identifies certain states and connects to outer detection systems

operators in the two-level systems A and B, respectively. Since the excitations are assumed to be fermionic excitons, and the optical near-field coupling  $U$  is considered a completely coherent process; this is explained in detail in Sect. 2. Energies for states are given as follows:

$${}_s\langle 1|\hat{H}|1\rangle_s = \hbar(\Omega + U), \quad (8)$$

$${}_a\langle 1|\hat{H}|1\rangle_a = \hbar(\Omega - U), \quad (9)$$

$${}_p\langle 2|\hat{H}|2\rangle_p = 2\hbar\Omega. \quad (10)$$

Equations (8) and (9) indicate that the energies of the coupled states,  $|1\rangle_s$  and  $|1\rangle_a$ , depend on the strength of optical near-field coupling,  $U$ , and differences in the energy from the two-level system have opposite contributions in each state. In the two-exciton states in (10), energy apparently degenerates because both systems are completely filled. These properties are useful for selective energy transfer in nanophotonic devices; sequential logic operations can be realized by using the excitation number dependence in this system.

Figure 4 schematically illustrates how the above selectivity represents a concept that is fundamental to nanophotonic devices. In the device, quantum mechanical and classical parts coexist; some characteristic excited states are created in the quantum mechanical part, and in order to connect a signal to an outer detection system, these states must then be selectively extracted from quantum mechanical part to classical dissipative one. This process is key to driving the nanophotonic device. Functional operations based on such conceptual structures are discussed in Sect. 4.

## 2 Optical Near-Field Coupling

In this section, we give a full account of energy transfer between locally excited states via an optical near field. From our theoretical treatment of optical near-field coupling, the readers will understand why dipole-inactive energy transfer

for far-field light changes allowed transition in the case of the optical near field. Concrete numerical results of coupling strength in a CuCl quantum-dot system are also provided, where the coupling strength determines operation speed of nanophotonic devices discussed in Sects. 3 and 4.

## 2.1 Theoretical Descriptions of an Optical Near Field

There are two ways to describe light–matter interaction theoretically; one is to use the minimal coupling Hamiltonian  $\mathbf{p} \cdot \mathbf{A}$  [9],  $\mathbf{p}$  being the electronic momentum and  $\mathbf{A}$  the vector potential, and the other is to use the multipolar QED Hamiltonian [10, 11] in the dipole approximation,  $\boldsymbol{\mu} \cdot \mathbf{D}$ , where  $\boldsymbol{\mu}$  and  $\mathbf{D}$  represent the electric dipole moment and electric displacement field, respectively. The two descriptions of light–matter interaction are connected by Power-Zienau–Woolley transformation [12], which is a unitary transformation of the Coulomb-gauge Hamiltonian. Here, the multipolar QED Hamiltonian is used because there are several advantages in the multipolar QED; first of all, it does not contain any explicit intermolecular or interquantum-dot Coulomb interactions in the interaction Hamiltonian and entire contribution to the fully retarded result is from the exchange of transverse photons, while in the minimal coupling, the intermolecular interactions arise both from the exchange of transverse photons, which include static components, and from the instantaneous intermolecular electrostatic interactions [13]. Second, it clarifies physical interpretation of the dipole inactive transition via the optical near field as we will discuss later.

Since our purpose of discussions is to propose and investigate nanophotonic solid devices, in the following, nanometric objects are assumed as quantum dots with discrete energy levels. In order to explain an extremely important feature in nanophotonics, internal electronic structures in a quantum dot are regarded as a collection of local dipoles, which is convenient to express the interactions between nanometric objects and an optical near field spatially distributed in nanometric space. We can also depict a dipole in one-body problem by using an effective mass approximation. Such theoretical approach has already been published [14] where the enhancement of electric quadrupole coupling was pointed out by assuming steep variation of electric field due to the optical near field. This phenomenon is equivalent to our result of the dipole-inactive transition, but in our theoretical formulation, in which field variation is caused by the coupling between the local dipoles in the neighboring quantum-dot pair, it is easy to obtain a physical interpretation.

In Sect. 2.2 interaction Hamiltonian is provided in the second-quantized form in terms of electron basis functions satisfying the quantum-dot boundary conditions, as well as transition dipole moments of excitons, and then, optical near-field coupling is derived on the basis of the projection operator method which is explained in Sect. 2.3.

## 2.2 Excitation and Transition in a Quantum Dot

### Interaction Hamiltonian

According to the dipole coupling in the multipolar QED Hamiltonian, the interaction between photons and nanometric materials can be written as [11]

$$\hat{H}_{\text{int}} = - \int \psi^\dagger(\mathbf{r}) \boldsymbol{\mu}(\mathbf{r}) \psi(\mathbf{r}) \cdot \hat{\mathbf{D}}(\mathbf{r}) d\mathbf{r} , \quad (11)$$

where  $\psi^\dagger(\mathbf{r})$  and  $\psi(\mathbf{r})$  denote field operators for electron creation and annihilation, respectively, and the dipole moment and the second-quantized electric displacement vector at position  $\mathbf{r}$  are expressed as  $\boldsymbol{\mu}(\mathbf{r})$  and  $\hat{\mathbf{D}}(\mathbf{r})$ , respectively. In a quantum dot, the electron field operators should be expanded in terms of basis functions  $\phi_{\nu\mathbf{n}}(\mathbf{r})$  that satisfy the electron boundary conditions in a quantum dot, that is analogy to those in bulk materials where the Bloch functions satisfying periodic boundary condition are used. The field operators are given by

$$\psi(\mathbf{r}) = \sum_{\nu=\text{c,v}} \sum_{\mathbf{n}} \hat{c}_{\nu\mathbf{n}} \phi_{\nu\mathbf{n}}(\mathbf{r}) , \quad (12)$$

$$\psi^\dagger(\mathbf{r}) = \sum_{\nu=\text{c,v}} \sum_{\mathbf{n}} \hat{c}_{\nu\mathbf{n}}^\dagger \phi_{\nu\mathbf{n}}^*(\mathbf{r}) , \quad (13)$$

where  $\hat{c}_{\nu\mathbf{n}}^\dagger$  and  $\hat{c}_{\nu\mathbf{n}}$  represent the creation and annihilation operators for the electrons specified by  $(\nu, \mathbf{n})$ , respectively, and the indices  $\nu = \text{c, v}$  denote the conduction and valence bands. The discrete energy levels in the quantum dot are labeled  $\mathbf{n}$ . The basis functions satisfy the following completeness condition, as well as orthonormalization:

$$\sum_{\nu=\text{c,v}} \sum_{\mathbf{n}} \phi_{\nu\mathbf{n}}^*(\mathbf{r}) \phi_{\nu\mathbf{n}}(\mathbf{r}') = \delta(\mathbf{r} - \mathbf{r}') . \quad (14)$$

Simultaneously, we express the electric displacement vector  $\hat{\mathbf{D}}(\mathbf{r})$  using exciton-polariton creation and annihilation operators  $(\hat{\xi}_{\mathbf{k}}^\dagger, \hat{\xi}_{\mathbf{k}})$ , where branch suffix of the exciton-polariton is suppressed by taking only an upper branch. We consider exciton-polaritons because a nanometric system in a near-field optical environment is always surrounded by macroscopic materials, such as the substrate, matrix, fiber probe, and so on. Previously [15,16], we proposed an effective interaction for such a nanometric system mediated by exciton-polaritons that exists in mixed states between photons and macroscopic material excitations instead of free photons. We showed that such a treatment provides a good description of the characteristics of an optical near field [17]. Using this, the electric displacement vector  $\hat{\mathbf{D}}(\mathbf{r})$  in (11) can be written as [18]

$$\hat{\mathbf{D}}(\mathbf{r}) = i \sqrt{\frac{2\pi}{V}} \sum_{\mathbf{k}} \sum_{\lambda=1}^2 e_{\lambda}(\mathbf{k}) f(k) (\hat{\xi}_{\mathbf{k}} e^{i\mathbf{k} \cdot \mathbf{r}} - \hat{\xi}_{\mathbf{k}}^\dagger e^{-i\mathbf{k} \cdot \mathbf{r}}) \quad (15)$$



with

$$f(k) = \frac{\hbar ck}{\sqrt{E(k)}} \sqrt{\frac{E^2(k) - E_m^2}{2E^2(k) - E_m^2 - \hbar^2 c^2 k^2}} , \quad (16)$$

where  $\hbar$ ,  $V$ ,  $\mathbf{e}_\lambda(\mathbf{k})$ , and  $\mathbf{k}$  are the Dirac constant, the quantization volume, the unit polarization vector, and the wavevector of the exciton-polaritons, respectively. Here we assume  $\mathbf{e}_\lambda(\mathbf{k})$  as real. The speed of light in a vacuum is  $c$ , and the exciton-polariton energy with a wavevector  $\mathbf{k}$  and the macroscopic material excitation energy are  $E(\mathbf{k})$  and  $E_m$ , respectively. Substituting (12) and (15) into (11) gives the interaction Hamiltonian in the second-quantized representation as

$$\hat{H}_{\text{int}} = \sum_{\nu \mathbf{n} \nu' \mathbf{n}' \mathbf{k} \lambda} (\hat{c}_{\nu \mathbf{n}}^\dagger \hat{c}_{\nu' \mathbf{n}'} \hat{\xi}_{\mathbf{k}} g_{\nu \mathbf{n} \nu' \mathbf{n}' \mathbf{k} \lambda} - \hat{c}_{\nu \mathbf{n}}^\dagger \hat{c}_{\nu' \mathbf{n}'} \hat{\xi}_{\mathbf{k}}^\dagger g_{\nu \mathbf{n} \nu' \mathbf{n}' - \mathbf{k} \lambda}) \quad (17)$$

with

$$g_{\nu \mathbf{n} \nu' \mathbf{n}' \mathbf{k} \lambda} = -i \sqrt{\frac{2\pi}{V}} f(k) \int \phi_{\nu \mathbf{n}}^*(\mathbf{r}) (\boldsymbol{\mu}(\mathbf{r}) \cdot \mathbf{e}_\lambda(\mathbf{k})) e^{i\mathbf{k} \cdot \mathbf{r}} \phi_{\nu' \mathbf{n}'}(\mathbf{r}) d\mathbf{r} . \quad (18)$$

### Transition Matrix Element for Exciton States

In order to describe the creation and annihilation of excitons in a quantum dot, it is convenient to use the Wannier representation in which electrons are localized in an atomic site  $\mathbf{R}$ . Then, the electron field operators can be expanded using the Wannier functions  $w_{\nu \mathbf{R}}(\mathbf{r})$  instead of  $\phi_{\nu \mathbf{n}}(\mathbf{r})$

$$\psi(\mathbf{r}) = \sum_{\nu=c,v} \sum_{\mathbf{R}} \hat{c}_{\nu \mathbf{R}} w_{\nu \mathbf{R}}(\mathbf{r}) , \quad \psi^\dagger(\mathbf{r}) = \sum_{\nu=c,v} \sum_{\mathbf{R}} \hat{c}_{\nu \mathbf{R}}^\dagger w_{\nu \mathbf{R}}^*(\mathbf{r}) , \quad (19)$$

where  $\hat{c}_{\nu \mathbf{R}}^\dagger$  and  $\hat{c}_{\nu \mathbf{R}}$  denote the creation and annihilation operators of electrons at site  $\mathbf{R}$  in the energy band  $\nu$ . These operators in the Wannier representation are written in terms of  $\hat{c}_{\nu \mathbf{n}}$  and  $\hat{c}_{\nu \mathbf{n}}^\dagger$  in (12) as follows:

$$\hat{c}_{\nu \mathbf{R}} = \sum_{\nu'=c,v} \sum_{\mathbf{n}} \hat{c}_{\nu' \mathbf{n}} \int w_{\nu \mathbf{R}}^*(\mathbf{r}) \phi_{\nu' \mathbf{n}}(\mathbf{r}) d\mathbf{r} , \quad (20)$$

$$\hat{c}_{\nu \mathbf{R}}^\dagger = \sum_{\nu'=c,v} \sum_{\mathbf{n}} \hat{c}_{\nu' \mathbf{n}}^\dagger \int w_{\nu \mathbf{R}}(\mathbf{r}) \phi_{\nu' \mathbf{n}}^*(\mathbf{r}) d\mathbf{r} . \quad (21)$$

When we assume excitons in the weak-confinement regime, i.e., an exciton Bohr radius to be smaller than the quantum-dot size, the exciton states in a quantum dot specified by the quantum number  $\mathbf{m}$  and  $\mu$  can be described by superposition of the excitons in the Wannier representation as [19]

$$\begin{aligned} |\Phi_{\mathbf{m}\mu}\rangle &= \sum_{\mathbf{R}, \mathbf{R}'} F_{\mathbf{m}}(\mathbf{R}_{\text{CM}}) \varphi_\mu(\boldsymbol{\beta}) \hat{c}_{c\mathbf{R}}^\dagger \hat{c}_{v\mathbf{R}} |\Phi_g\rangle \\ &= \sum_{\mathbf{R}, \mathbf{R}'} F_{\mathbf{m}}(\mathbf{R}_{\text{CM}}) \varphi_\mu(\boldsymbol{\beta}) \sum_{\mathbf{n}, \mathbf{n}'} h_{\mathbf{R}\mathbf{n}\mathbf{R}'\mathbf{n}'} \hat{c}_{c\mathbf{n}}^\dagger \hat{c}_{v\mathbf{n}'} |\Phi_g\rangle , \end{aligned} \quad (22)$$

where  $F_{\mathbf{m}}(\mathbf{R}_{\text{CM}})$  and  $\varphi_{\mu}(\boldsymbol{\beta})$  denote the envelope functions for the center of mass and relative motions of the excitons, respectively. These are  $\mathbf{R}_{\text{CM}} = (m_e \mathbf{R}' + m_h \mathbf{R})/(m_e + m_h)$  and  $\boldsymbol{\beta} = \mathbf{R}' - \mathbf{R}$ , where  $m_e$  and  $m_h$  are the effective masses of the electrons and holes. The overlap integrals  $h_{\mathbf{R}\mathbf{n}\mathbf{R}'\mathbf{n}'}$  are defined as

$$h_{\mathbf{R}\mathbf{n}\mathbf{R}'\mathbf{n}'} = \iint w_{\mathbf{v}\mathbf{R}}^*(\mathbf{r}_2) w_{\mathbf{c}\mathbf{R}'}(\mathbf{r}_1) \phi_{\mathbf{c}\mathbf{n}}^*(\mathbf{r}_1) \phi_{\mathbf{v}\mathbf{n}'}(\mathbf{r}_2) d\mathbf{r}_1 d\mathbf{r}_2. \quad (23)$$

The sum of  $\nu'$  in (20) is determined automatically as  $\hat{c}_{\mathbf{c}\mathbf{n}}^\dagger$  and  $\hat{c}_{\mathbf{v}\mathbf{n}'}$  because the valence band is fully occupied in the initial ground state  $|\Phi_g\rangle$ . Using (17) and (22), the transition matrix element from the exciton state to the ground state is obtained as

$$\begin{aligned} \langle \Phi_g | \hat{H}_{\text{int}} | \Phi_{\mathbf{m}\mu} \rangle &= \sum_{\mathbf{n}_1, \mathbf{n}_2} \sum_{\mathbf{R}, \mathbf{R}'} F_{\mathbf{m}}(\mathbf{R}_{\text{CM}}) \varphi_{\mu}(\boldsymbol{\beta}) \\ &\times \sum_{\mathbf{k}} \sum_{\lambda=1}^2 (\hat{\xi}_{\mathbf{k}} g_{\mathbf{v}\mathbf{n}_1 \mathbf{c}\mathbf{n}_2 \mathbf{k}\lambda} - \hat{\xi}_{\mathbf{k}}^\dagger g_{\mathbf{v}\mathbf{n}_1 \mathbf{c}\mathbf{n}_2 - \mathbf{k}\lambda}) h_{\mathbf{R}\mathbf{n}_2 \mathbf{R}'\mathbf{n}_1}, \end{aligned} \quad (24)$$

where we use the following relation:

$$\langle \Phi_g | \hat{c}_{\mathbf{v}\mathbf{n}_1}^\dagger \hat{c}_{\mathbf{c}\mathbf{n}_2} \hat{c}_{\mathbf{c}\mathbf{n}_3}^\dagger \hat{c}_{\mathbf{v}\mathbf{n}_4} | \Phi_g \rangle = \delta_{\mathbf{n}_1, \mathbf{n}_4} \delta_{\mathbf{n}_2, \mathbf{n}_3}. \quad (25)$$

In addition, with the help of the completeness and orthonormalization of  $\phi_{\nu\mathbf{n}}(\mathbf{r})$  [see (14)], we can simplify the product of  $g$  and  $h$  as

$$\begin{aligned} \sum_{\mathbf{n}_1, \mathbf{n}_2} g_{\mathbf{v}\mathbf{n}_1 \mathbf{c}\mathbf{n}_2 \mathbf{k}\lambda} h_{\mathbf{R}\mathbf{n}_2 \mathbf{R}'\mathbf{n}_1} &= -i \sqrt{\frac{2\pi}{V}} f(k) \int w_{\mathbf{v}\mathbf{R}}^*(\mathbf{r}) \boldsymbol{\mu}(\mathbf{r}) w_{\mathbf{c}\mathbf{R}'}(\mathbf{r}) \cdot \mathbf{e}_{\lambda}(\mathbf{k}) e^{i\mathbf{k} \cdot \mathbf{r}} d\mathbf{r} \\ &\approx -i \sqrt{\frac{2\pi}{V}} f(k) (\boldsymbol{\mu}_{\text{cv}} \cdot \mathbf{e}_{\lambda}(\mathbf{k})) e^{i\mathbf{k} \cdot \mathbf{R}} \delta_{\mathbf{R}, \mathbf{R}'}, \end{aligned} \quad (26)$$

where the transformation of the spatial integral in the first line of (26) into the sum of the unit cells and the spatial localization of the Wannier functions provides  $\delta_{\mathbf{R}, \mathbf{R}'}$  in the second line. The transition dipole moment for each unit cell is defined as

$$\boldsymbol{\mu}_{\text{cv}} = \int_{\text{UC}} w_{\mathbf{v}\mathbf{R}}^*(\mathbf{r}) \boldsymbol{\mu}(\mathbf{r}) w_{\mathbf{c}\mathbf{R}}(\mathbf{r}) d\mathbf{r}. \quad (27)$$

We assume that the transition dipole moment is the same as that of the bulk material, independent of the site  $\mathbf{R}$ , and that the electric displacement vector is uniform at each site. Finally, (24) is reduced to

$$\begin{aligned} \langle \Phi_g | \hat{H}_{\text{int}} | \Phi_{\mathbf{m}\mu} \rangle &= -i \sqrt{\frac{2\pi}{V}} \sum_{\mathbf{R}} \sum_{\mathbf{k}} \sum_{\lambda=1}^2 f(k) (\boldsymbol{\mu}_{\text{cv}} \cdot \mathbf{e}_{\lambda}(\mathbf{k})) F_{\mathbf{m}}(\mathbf{R}) \varphi_{\mu}(0) \\ &\times \left( \hat{\xi}_{\mathbf{k}} e^{i\mathbf{k} \cdot \mathbf{R}} - \hat{\xi}_{\mathbf{k}}^\dagger e^{-i\mathbf{k} \cdot \mathbf{R}} \right). \end{aligned} \quad (28)$$

Here, we note that the exciton-polariton field expanded by the plane wave with the wavevector  $\mathbf{k}$  depends on the site  $\mathbf{R}$  in the quantum dot because we do not apply the long wave approximation that is usually used for far-field light.

### 2.3 Optical Near-Field Coupling Between Quantum Dots

#### Formulation

Until now, we have derived the transition matrix element from the exciton state to the ground state in a quantum dot. Considering operations of nanophotonic devices, signal carrier corresponds to the energy transfer between nanometric objects, or quantum dots, which are electronically separated, and the speed of the energy transfer is determined by the coupling strength of an optical near field. In this stage, we derive the coupling strength

$$\hbar U = \langle \Psi_f | \hat{H}_{\text{int}} | \Psi_i \rangle, \quad (29)$$

where  $|\Psi_i\rangle$  and  $|\Psi_f\rangle$  represent exact initial and final states, respectively, in which the states consist of quantum-dot states, photon fields, and some external degrees of freedom, such as a substrate and a glass fiber probe. Since the exact states cannot be given rigorously, we deal with the problem for taking the minimum matter and photon states by using the projection operator method, where the theoretical treatment in such complex system comes down to two-body problem as we have reported in detail [16, 20].

We can rewrite the exact eigenstate as two substates which belong in a relevant P-space and an irrelevant Q-space, which are expressed by using projection operators  $P$  and  $Q$  as  $|\Psi_\lambda^P\rangle = P|\Psi_\lambda\rangle$  and  $|\Psi_\lambda^Q\rangle = Q|\Psi_\lambda\rangle$ , respectively, where  $\lambda = i, f$ . Here,  $P$  and  $Q$  are specified by the following relations:  $P + Q = 1$ ,  $P^2 = P$ ,  $Q^2 = Q$ ,  $P^\dagger = P$ , and  $Q^\dagger = Q$  [21]. In the case of two-quantum-dot system, P-space is constructed from the eigenstates of  $\hat{H}_0$ , i.e., a combination of the two energy levels for each quantum dot and the exciton-polariton vacuum state. In Q-space, which is complementary to P-space, the exciton-polariton states are not vacant. According to this notation, the exact state can be formally expressed by using the state in P-space only as

$$|\Psi_\lambda\rangle = \hat{J}P(P\hat{J}^\dagger\hat{J}P)^{-1/2}|\Psi_\lambda^P\rangle, \quad (30)$$

where

$$\hat{J} = \left[ 1 - (E_\lambda - \hat{H}_0)^{-1}Q\hat{H}_{\text{int}} \right]^{-1}, \quad (31)$$

and  $E_\lambda$  represents the eigenenergy of the total Hamiltonian  $\hat{H}$ . Using (30), we can obtain the effective interaction  $\hat{H}_{\text{eff}}$  as

$$\langle \Psi_f | \hat{H}_{\text{int}} | \Psi_i \rangle = \langle \Psi_f^P | \hat{H}_{\text{eff}} | \Psi_i^P \rangle, \quad (32)$$

where

$$\hat{H}_{\text{eff}} = (P\hat{J}^\dagger\hat{J}P)^{-1/2}(P\hat{J}^\dagger\hat{H}_{\text{int}}\hat{J}P)(P\hat{J}^\dagger\hat{J}P)^{-1/2}. \quad (33)$$

To evaluate further (32), we approximate operator  $\hat{J}$  and eigenvalue  $E_\lambda$  perturbatively with respect to  $\hat{H}_{\text{int}}$ ; that is,  $\hat{J} = 1 + (E_0^P - E_0^Q)^{-1}\hat{H}_{\text{int}} + \dots$ . Since the lowest order is  $\langle \Psi_f^P | P\hat{H}_{\text{int}}P | \Psi_i^P \rangle = 0$ , (32) is rewritten within the

second order as

$$\hbar U = \sum_m \left\langle \Psi_f^P | \hat{H}_{\text{int}} | m^Q \right\rangle \left\langle m^Q | \hat{H}_{\text{int}} | \Psi_i^P \right\rangle \left( \frac{1}{E_{0i}^P - E_{0m}^Q} + \frac{1}{E_{0f}^P - E_{0m}^Q} \right), \quad (34)$$

where  $E_{0i}^P$ ,  $E_{0f}^P$ , and  $E_{0m}^Q$  represent the eigenenergies of the unperturbed Hamiltonian for the initial and final states in P-space and the intermediate state in Q-space, respectively. Since we focus on the interdot interaction of (34), we set the initial and final states in P-space to  $|\Psi_i^P\rangle = |\Phi_{\mathbf{m}\mu}^A\rangle|\Phi_g^B\rangle|0\rangle$  and  $|\Psi_f^P\rangle = |\Phi_g^A\rangle|\Phi_{\mathbf{m}'\mu'}^B\rangle|0\rangle$ . Then, the intermediate states in Q-space that involve exciton-polaritons with the wavevector  $\mathbf{k}$  are utilized for the energy transfer from one quantum dot to the other, according to  $|m^Q\rangle = |\Phi_g^A\rangle|\Phi_g^B\rangle|\mathbf{k}\rangle$  and  $|\Phi_{\mathbf{m}\mu}^A\rangle|\Phi_{\mathbf{m}'\mu'}^B\rangle|\mathbf{k}\rangle$ . The superscripts A and B are used to label two quantum dots. Substituting (28), one can rewrite (34) as

$$\hbar U = \varphi_\mu^A(0)\varphi_{\mu'}^{B*}(0) \iint F_{\mathbf{m}}^A(\mathbf{R}_A) F_{\mathbf{m}'}^{B*}(\mathbf{R}_B) \times (Y_A(\mathbf{R}_A - \mathbf{R}_B) + Y_B(\mathbf{R}_A - \mathbf{R}_B)) d\mathbf{R}_A d\mathbf{R}_B, \quad (35)$$

where the sum of  $\mathbf{R}_\alpha$  ( $\alpha = A, B$ ) in (28) is transformed to the integral form. The functions  $Y_\alpha(\mathbf{R}_{AB})$ , which connect the two spatially isolated two envelope functions  $F_{\mathbf{m}}^A(\mathbf{R}_A)$  and  $F_{\mathbf{m}'}^B(\mathbf{R}_B)$ , are defined as

$$Y_\alpha(\mathbf{R}_{AB}) = -\frac{1}{4\pi^2} \sum_{\lambda=1}^2 \int (\boldsymbol{\mu}_{\text{cv}}^A \cdot \hat{\mathbf{e}}_\lambda(\mathbf{k})) (\boldsymbol{\mu}_{\text{cv}}^B \cdot \hat{\mathbf{e}}_\lambda(\mathbf{k})) f^2(k) \times \left( \frac{e^{i\mathbf{k} \cdot \mathbf{R}_{AB}}}{E(k) + E_\alpha} + \frac{e^{-i\mathbf{k} \cdot \mathbf{R}_{AB}}}{E(k) - E_\alpha} \right) d\mathbf{k}, \quad (36)$$

where  $\mathbf{R}_{AB} = \mathbf{R}_A - \mathbf{R}_B$  is used.

In order to obtain an explicit functional form of  $Y_\alpha(\mathbf{R}_{AB})$ , we apply the effective mass approximation to the exciton-polaritons

$$E(k) = \frac{\hbar^2 k^2}{2m_p} + E_m, \quad (37)$$

where  $m_p$  is the exciton-polariton effective mass. Using this approximation, (36) can be transformed into

$$Y_\alpha(\mathbf{R}_{AB}) = (\boldsymbol{\mu}_{\text{cv}}^A \cdot \boldsymbol{\mu}_{\text{cv}}^B) \left[ W_{\alpha+} e^{-\Delta_{\alpha+} R_{AB}} \left( \frac{\Delta_{\alpha+}^2}{R_{AB}} + \frac{\Delta_{\alpha+}}{R_{AB}^2} + \frac{1}{R_{AB}^3} \right) - W_{\alpha-} e^{-\Delta_{\alpha-} R_{AB}} \left( \frac{\Delta_{\alpha-}^2}{R_{AB}} + \frac{\Delta_{\alpha-}}{R_{AB}^2} + \frac{1}{R_{AB}^3} \right) \right] - (\boldsymbol{\mu}_{\text{cv}}^A \cdot \hat{\mathbf{R}}_{AB}) (\boldsymbol{\mu}_{\text{cv}}^B \cdot \hat{\mathbf{R}}_{AB}) \left[ W_{\alpha+} e^{-\Delta_{\alpha+} R_{AB}} \left( \frac{\Delta_{\alpha+}^2}{R_{AB}} + \frac{3\Delta_{\alpha+}}{R_{AB}^2} + \frac{3}{R_{AB}^3} \right) - W_{\alpha-} e^{-\Delta_{\alpha-} R_{AB}} \left( \frac{\Delta_{\alpha-}^2}{R_{AB}} + \frac{3\Delta_{\alpha-}}{R_{AB}^2} + \frac{3}{R_{AB}^3} \right) \right], \quad (38)$$

where  $R_{AB}$  and  $\hat{\mathbf{R}}_{AB}$  are the absolute value  $|\mathbf{R}_{AB}|$  and the unit vector defined by  $\mathbf{R}_{AB}/R_{AB}$ , respectively. The weight coefficients  $W_{\alpha\pm}$  and decay constants  $\Delta_{\alpha\pm}$  are given by

$$W_{\alpha\pm} = \frac{\sqrt{E_p}}{E_\alpha} \frac{(E_m - E_\alpha)(E_m + E_\alpha)}{(E_m - E_p \mp E_\alpha)(E_m \pm E_\alpha) - E_m^2/2}, \quad (39)$$

$$\Delta_{\alpha\pm} = \frac{1}{\hbar c} \sqrt{E_p(E_m \pm E_\alpha)}, \quad (40)$$

where the exciton-polariton effective mass is rewritten as  $E_p = m_p c^2$ . Since the dipole moments  $\mu_{cv}^A$  and  $\mu_{cv}^B$  are not determined as fixed values, we assume that they are parallel, and take a rotational average of (38). Therefore,  $\langle (\mu_{cv}^A \cdot \hat{\mathbf{R}}_{AB})(\mu_{cv}^B \cdot \hat{\mathbf{R}}_{AB}) \rangle = \mu_{cv}^A \mu_{cv}^B / 3$  with  $\mu_{cv}^\alpha = |\mu_{cv}^\alpha|$ , and we obtain the final form of the function  $Y_\alpha(R_{AB})$  as

$$Y_\alpha(R_{AB}) = \frac{2\mu_{cv}^A \mu_{cv}^B}{3R_{AB}} (W_{\alpha+} \Delta_{\alpha+}^2 e^{-\Delta_{\alpha+} R_{AB}} - W_{\alpha-} \Delta_{\alpha-}^2 e^{-\Delta_{\alpha-} R_{AB}}). \quad (41)$$

Equation (41) is the sum of two Yukawa functions with a short and long interaction range (heavy and light effective mass) given in (40). We can estimate the coupling strength between two quantum dots from the analytic form of the interaction potential given by (35) and (41), and we can show the existence of dipole-forbidden energy transfer driven by the optical near-field coupling, as discussed in the following.

## Numerical Results

In this section, we give typical values of the coupling strength of  $\hbar U$  in (35) using an example of CuCl quantum cubes embedded in an NaCl matrix. Due to the effect of size confinement, the center of mass motion and relative motion for an exciton in a CuCl quantum cube are [19]

$$F_{\mathbf{m}}^\alpha(\mathbf{R}_\alpha) = \left(\frac{2}{L_\alpha}\right)^{3/2} \sin\left(\frac{\pi m_x x_\alpha}{L_\alpha}\right) \sin\left(\frac{\pi m_y y_\alpha}{L_\alpha}\right) \sin\left(\frac{\pi m_z z_\alpha}{L_\alpha}\right), \quad (42)$$

$$\varphi_{1s}(r) = \frac{1}{\sqrt{\pi a^3}} e^{-r/a}, \quad (43)$$

respectively, where the atomic site and the quantum number are represented by  $\mathbf{R}_\alpha = (x_\alpha, y_\alpha, z_\alpha)$  with  $\alpha = A, B$  and  $\mathbf{m} = (m_x, m_y, m_z)$  with  $m_x, m_y, m_z = 1, 2, 3, \dots$ . The variables  $L_\alpha$  and  $a$  denote a width of the quantum cube and the Bohr radius of the exciton, respectively. Here, we assume relative motion in the 1s state. The coupling strength is obtained numerically by substituting (41) and (42) into (35). In Fig. 5a, the calculation results are plotted as a function of the intercube distance. The curve with square dots represents the coupling between the dipole-active exciton levels, i.e.,  $\mathbf{m} = \mathbf{m}' = (1, 1, 1)$ , in two quantum cubes. When we set the intercube distance and a width of the quantum cubes as  $d = 5$  nm and  $L_A = L_B = 10$  nm,

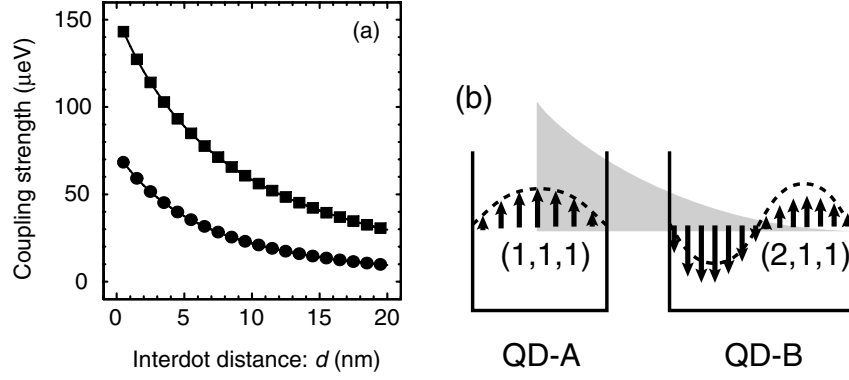


**Fig. 5.** (a) Coupling strength of the optical near field between pairs of CuCl quantum cubes embedded in an NaCl matrix. The curves shown with square and circular dots correspond to quantum numbers for the exciton center of mass motion  $\mathbf{m} = \mathbf{m}' = (1, 1, 1)$ , and  $\mathbf{m} = (1, 1, 1)$  and  $\mathbf{m}' = (2, 1, 1)$ , respectively. The energy level  $\mathbf{m}' = (2, 1, 1)$  is a dipole-inactive state for conventional far-field light. The parameters are set as  $E_A = E_B = 3.22$  eV,  $E_m = 6.9$  eV,  $\mu_{cv}^A = \mu_{cv}^B = 1.73 \times 10^{-2}$  eV,  $L_A = 10$  nm,  $L_B = 10$  and  $14.1$  nm ( $\mathbf{m}' = (1, 1, 1)$  and  $(2, 1, 1)$ ), and  $a = 0.67$  nm. (b) Schematic illustration of a transition between dipole-active and dipole-inactive states via the optical near-field coupling. Steeply gradient optical near field enables to excite near side local dipoles in a quantum dot with dipole-inactive  $(2, 1, 1)$ -level

respectively, the coupling strength is about  $89 \mu\text{eV}$  ( $U^{-1} = 7.4$  ps). The curve with circular dots is the result for  $\mathbf{m} = (1, 1, 1)$  and  $\mathbf{m}' = (2, 1, 1)$ . For conventional far-field light,  $\mathbf{m}' = (2, 1, 1)$  is the dipole-inactive exciton level, and it follows that the optical near-field interaction inherently involves such a transition because of the finite interaction range. Figure 5b is a schematic illustration of the dipole-inactive transition, in which the optical near field enables to excite the local dipoles at the near side in a quantum dot with dipole-inactive level for far-field light. This coupling strength is estimated from Fig. 5a as  $\hbar U = 37 \mu\text{eV}$  ( $U^{-1} = 17.7$  ps) for  $d = 5$  nm, and  $\hbar U = 14 \mu\text{eV}$  ( $U^{-1} = 46.9$  ps) for  $d = 15$  nm, where the cube sizes are set as  $L_A = 10$  nm and  $L_B = 14.1$  nm to realize resonant energy transfer between the exciton state in QD-A and the first exciton excitation state in QD-B. The coupling strength ( $\mathbf{m} \neq \mathbf{m}'$ ) is approximately half that of  $\mathbf{m} = \mathbf{m}'$  at the same intercube distance, but it is strong enough for our proposed nanophotonic devices. For functional operations, the difference between the coupling strengths is important to divide the system into two parts, i.e., a quantum mechanical part and a classical dissipative part, as illustrated in Fig. 4.

## 2.4 Summary

In this section, we formulate a optical near-field coupling by using appropriate bases which are constructed from typical excitonic states in a quantum dot and

exciton–polariton state in a surrounding system, and not using the long wave approximation which often applies to a conventional optical interaction in an atomic system. Although we have derived the coupling in the lowest order as given in (34), our formulation would be exact if we take rigorous eigenstate of exciton–polaritons as the intermediate states, instead of the simple effective mass approximation which is applied in the above discussion. However, in the following sections, our interests are characteristic functional operations of nanophotonic devices on the basis of certain coupling strength of the optical near field, rather than to understand fundamental properties of optical near-field coupling. More rigorous description of the optical near-field coupling will discuss elsewhere.

From numerical results shown in Fig. 5, the coupling strength of optical near field depends on the interdot distance, which is one of key features for nanophotonic device operations. By using this, we can control the dynamics of energy flow in nanometric space and develop some functional operations inherent to nanophotonic devices. Furthermore, we showed that dipole inactive energy transfer can occur when a distance between isolated quantum systems becomes enough small, which is related to the energy states in nanometric objects as well as steeply gradient spatial distribution of the optical near field. Especially, the dipole-inactive energy transfer between the states with different quantum numbers enables to realize unidirectional energy transfer in a nanometric system with the help of fast relaxation of exciton sublevels. This is a quite important feature for signal isolation in nanophotonic devices. In Sects. 3 and 4, we discuss operation principles of various functional devices by using such features of the optical near-field coupling skillfully.

### 3 Nanophotonic Switch Based on Dissipation Control

In Sect. 2, we had theoretically explained that an exciton in a dipole-inactive energy level can be excited by using an optical near field. A relaxation time of the exciton in the dipole-inactive level, the higher energy sublevel, is generally in the order of a few ps because of the strong coupling between an exciton and a phonon reservoir in a surrounding system [22]. Since the coupling strength of the optical near field corresponds to about subhundred ps, which has been estimated in Sect. 2, the intra-sublevel relaxation is as a figure fast as in the order of energy transfer between two quantum dots. Therefore, unidirectional energy transfer can be realized in a two or more quantum-dot system by mediating the intra-sublevel relaxation. On the other hand, we can create and annihilate an exciton in an exciton ground state by using external pumping light. Excitons in a quantum-dot system affect exciton–exciton interaction in a quantum dot, because more than an exciton confined to nanometric space. We have qualitatively regarded the excitons as fermionic particles, that is of course exact. When the lowest energy sublevel is occupied, the exciton population cannot drop into the lowest energy level,

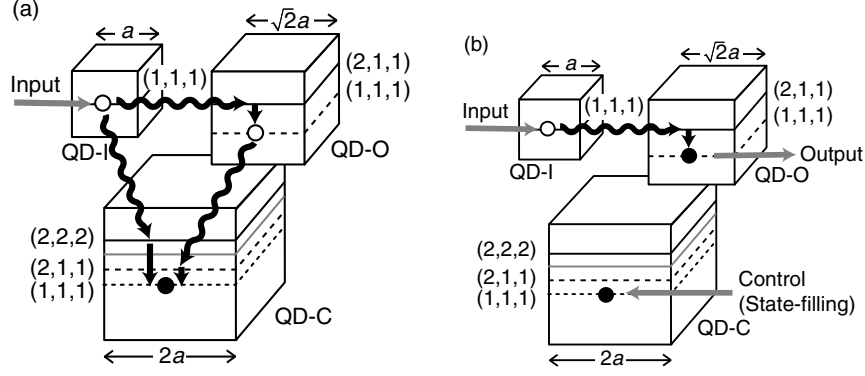


**Fig. 6.** A nanophotonic switch consisting of three quantum cubes with discrete energy levels showing the (a) OFF- and (b) ON-states

and thus, we can change the dissipation path selectively by arranging several quantum dots. This selectivity reads the origin of a nanophotonic switching operation.

In this section, we investigate our proposed nanophotonic switch, which is a basic element of nanophotonic devices [23]. Figure 6 illustrates a switch that consists of three quantum dots (cubes) with discrete exciton energy levels depending on the quantum-dot size. The one-side lengths of these cubes are chosen in the ratio  $1:\sqrt{2}:2$ , so that the adjacent quantum dots have resonant energy levels. The principle of operation of the switch is as follows: as shown in Fig. 6a, an exciton or population is created at the  $(1, 1, 1)$ -level in QD-I as an initial condition. Then the population is transferred to QD-O and QD-C as a result of an optical near-field coupling. Owing to the fast relaxation between sublevels in each dot via exciton-phonon coupling, the population is transferred to lower energy levels, and finally collected at the lowest  $(1, 1, 1)$ -level in QD-C. This corresponds to the OFF-state of the switch, and, consequently, we obtain no output signals from the output port, i.e., the  $(1, 1, 1)$ -level in QD-O. By contrast, in the ON-state of the switch (Fig. 6b), the  $(1, 1, 1)$ -level in QD-C is initially filled by the control light, isolating QD-C from the other two quantum dots. The input population only reaches the  $(1, 1, 1)$ -level in QD-O and can be detected as output signals, either by the optical near-field coupling to the detector or by far-field light emitted with electron-hole recombination.

From the above explanation, we understand that the key parameters determining the response time of the device are the coupling strength between two quantum dots via an optical near fields, and that between excitons and a phonon reservoir. In Sect. 3.1, dynamics of exciton population is formulated on the basis of quantum mechanical density matrix formalism, where we consider the phonon field as well as the optical near field discussed in Sect. 2, and roles of some key parameters in such a quantum-dot system are numerically clarified. This allows us to discuss the temporal dynamics of our proposed



nanophotonic. We evaluate the response time of the CuCl quantum-cube system as a numerical example, which have been extensively examined in experimental and theoretical studies of quantum dots [19, 22, 24, 25]. Section 3.2 devotes to evaluate switching operations in a three quantum-dot system as shown in Fig. 6, where the effect of state-filling is introduced phenomenologically. Furthermore, faster iterative switching operations can be achieved in the order of 100 ps, when we apply appropriate control light pulse for utilizing stimulated absorption and emission effectively, which will be discussed by means of numerical analysis in Sect. 3.3.

### 3.1 Dynamics in a Two-Quantum-Dot System with Dissipation

As mentioned above, relaxation in the exciton sublevels guarantees the unidirectional energy transfer in a system with several quantum dots. The relaxation originates from coupling between exciton excited state and lattice vibrations in a quantum dot and surrounding matter which are regarded as a phonon reservoir. In order to understand energy transfer dynamics in such a quantum-dot system, which goes through a dissipative process, we first examine a two-quantum-dot system coupled to the phonon reservoir.

#### Formulation

In Fig. 7, we schematically illustrate a considered two-quantum-dot system and a phonon reservoir system, in which all energy transfer paths are depicted except for the coupling to far-field light because of different time scales. The Hamiltonian of the system is modeled as

$$\hat{H} = \hat{H}_0 + \hat{H}_{\text{int}} + \hat{H}_{\text{SR}} \quad (44)$$

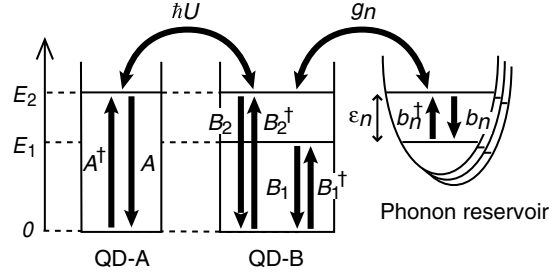


**Fig. 7.** Two-quantum-dot system. QD-A and QD-B are resonantly coupled due to an optical near-field interaction, and the sublevels in QD-B are coupled with the phonon reservoir

and

$$\hat{H}_0 = \hbar\Omega_2\hat{A}^\dagger\hat{A} + \hbar\Omega_1\hat{B}_1^\dagger\hat{B}_1 + \hbar\Omega_2\hat{B}_2^\dagger\hat{B}_2 + \hbar\sum_n\omega_n\hat{b}_n^\dagger\hat{b}_n, \quad (45)$$

$$\hat{H}_{\text{int}} = \hbar U(\hat{A}^\dagger\hat{B}_2 + \hat{B}_2^\dagger\hat{A}), \quad (46)$$

$$\hat{H}_{\text{SR}} = \hbar\sum_n(g_n\hat{b}_n^\dagger\hat{B}_1^\dagger\hat{B}_2 + g_n^*\hat{b}_n\hat{B}_2^\dagger\hat{B}_1). \quad (47)$$

When we assume that initial and final states are constructed only in terms of one-exciton states, the creation (annihilation) operators of excitons can be written as follows:  $\hat{A}^\dagger = [|e\rangle\langle g|]_A$  ( $\hat{A} = [|g\rangle\langle e|]_A$ ),  $\hat{B}_1^\dagger = [|e\rangle\langle g|]_{B_1}$ , ( $\hat{B}_1 = [|g\rangle\langle e|]_{B_1}$ ), and  $\hat{B}_2^\dagger = [|e\rangle\langle g|]_{B_2}$ , ( $\hat{B}_2 = [|g\rangle\langle e|]_{B_2}$ ). We can easily understand the following commutation relations:  $[\hat{B}_i^\dagger, \hat{B}_j] = \delta_{i,j}([|e\rangle\langle e|]_{B_i} - [|g\rangle\langle g|]_{B_i})$  and  $[\hat{B}_i, \hat{B}_j] = [\hat{B}_i^\dagger, \hat{B}_j^\dagger] = 0$  ( $i, j = 1, 2$ ). Therefore, the operators are neither bosonic nor fermionic. Bosonic operators ( $\hat{b}_n^\dagger, \hat{b}_n$ ) are for the phonons with eigenenergy  $\hbar\omega_n$ . For simplicity, the rotating wave approximation is used in the interaction Hamiltonian  $\hat{H}_{\text{int}}$  as  $(\hat{A} + \hat{A}^\dagger)(\hat{B}_2 + \hat{B}_2^\dagger) \approx \hat{A}^\dagger\hat{B}_2 + \hat{A}\hat{B}_2^\dagger$ . Phonon reservoir is assumed to be a collection of multiple harmonic oscillators labeled  $n$ . Note that the exciton-polariton degrees of freedom have already been traced out, and thus the coupling strength of the optical near field,  $\hbar U$ , appears in (46). Dynamics of an exciton in this system is given by the following Liouville equation [26, 27]

$$\dot{\hat{\rho}}(t) = -\frac{i}{\hbar}[\hat{H}, \hat{\rho}(t)], \quad (48)$$

where  $\hat{\rho}(t)$  represents the density operator, traced out the exciton-polariton degrees of freedom. In order to express the second-order temporal correlation clearly, the formal solution of (48) in the integral form is again substituted into the right-hand side of (48), and thus

$$\begin{aligned} \dot{\hat{\rho}}^{\text{I}}(t) = & -\frac{i}{\hbar} \left[ \hat{H}_{\text{int}} + \hat{H}_{\text{SR}}^{\text{I}}(t), \hat{\rho}^{\text{I}}(0) \right] \\ & - \frac{1}{\hbar^2} \int_0^t \left[ \hat{H}_{\text{int}} + \hat{H}_{\text{SR}}^{\text{I}}(t), \left[ \hat{H}_{\text{int}} + \hat{H}_{\text{SR}}^{\text{I}}(t'), \hat{\rho}^{\text{I}}(t') \right] \right] dt', \end{aligned} \quad (49)$$

where the superscript I means the interaction picture, and the relation  $\hat{H}_{\text{int}}^{\text{I}}(t) = \hat{H}_{\text{int}}$  is used [26]. Since we are interested in the exciton population in the two-quantum-dot system, we take a trace with respect to the degrees of freedom of the phonon reservoir as  $\hat{\rho}_S^{\text{I}}(t) = \text{Tr}_R[\hat{\rho}^{\text{I}}(t)]$ . Here, the density operator is assumed to be a direct product of the quantum-dot system part  $\hat{\rho}_S^{\text{I}}(t)$  and the reservoir system part  $\hat{\rho}_R^{\text{I}}(t)$ . If the reservoir has a very large volume, deviation from the initial value can be neglected, and the density operator is approximated as

$$\hat{\rho}^{\text{I}}(t) = \hat{\rho}_S^{\text{I}}(t)\hat{\rho}_R^{\text{I}}(t) \approx \hat{\rho}_S^{\text{I}}(t)\hat{\rho}_R(0), \quad (50)$$

which corresponds to the Born approximation [26]. Taking a trace on both sides of (49) about the reservoir operator, we obtain

$$\begin{aligned}
\dot{\hat{\rho}}_S^I(t) = & -iU(r)[\hat{A}^\dagger \hat{B}_2 + \hat{B}_2^\dagger \hat{A}] \\
& - \sum_n n(\omega_n, T) \left[ (\{\hat{C} \hat{C}^\dagger, \hat{\rho}_S^I(t)\} - 2\hat{C}^\dagger \hat{\rho}_S^I(t) \hat{C}) \otimes \gamma_n^r(t) \right. \\
& \quad \left. - i[\hat{C} \hat{C}^\dagger, \hat{\rho}_S^I(t)] \otimes \gamma_n^i(t) \right] \\
& - \sum_n [1 + n(\omega_n, T)] \left[ (\{\hat{C}^\dagger \hat{C}, \hat{\rho}_S^I(t)\} - 2\hat{C} \hat{\rho}_S^I(t) \hat{C}^\dagger) \otimes \gamma_n^r(t) \right. \\
& \quad \left. + i[\hat{C}^\dagger \hat{C}, \hat{\rho}_S^I(t)] \otimes \gamma_n^i(t) \right], \tag{51}
\end{aligned}$$

where the curly brackets  $\{\cdot\}$  represent the anti-commutation relation, and the notation  $\otimes$  designates the convolution integral. In order to avoid verbose expression, we make the following replacement:  $\hat{C}^\dagger = \hat{B}_2^\dagger \hat{B}_1$  and  $\hat{C} = \hat{B}_1^\dagger \hat{B}_2$ . Since we assume that the reservoir system is at equilibrium, the terms including  $\text{Tr}_R[\hat{b}_n^\dagger \hat{\rho}_R(0)]$  and  $\text{Tr}_R[\hat{b}_n \hat{\rho}_R(0)]$  disappear in (51). The number of phonons in the equilibrium state is written as  $n(\omega_n, T) = \text{Tr}_R[\hat{b}_n^\dagger \hat{b}_n \hat{\rho}_R(0)]$ , and it follows Bose–Einstein statistics as

$$n(\omega_n, T) = \frac{1}{e^{\hbar\omega_n/k_B T} - 1}. \tag{52}$$

The real and imaginary parts of function

$$\gamma_n(t) = |g_n|^2 e^{i(\Delta\omega - \omega_n)t} \tag{53}$$

with  $\hbar\omega = \hbar(\Omega_2 - \Omega_1)$  are represented as  $\gamma_n^r(t)$  and  $\gamma_n^i(t)$ , respectively, and are related to the relaxation (real part) and energy shift (imaginary part) of the energy level in QD-B that is originated from the coupling to the phonon reservoir. The convolution integral in (51) expresses a memory effect due to time delay in the phonon reservoir. However, if the dynamics of the reservoir system are much faster than those of the two-quantum-dot system, one can approximate the density operator of the two-dot system as  $\hat{\rho}_S^I(t - t') = \hat{\rho}_S^I(t)$  (a Markov approximation). Using this approximation, and rewriting the summation as  $\sum_n = \int_0^\infty D(\omega) d\omega$ , with  $D(\omega)$  being the density of states for each phonon, we can express the convolution integral analytically as

$$\begin{aligned}
& \sum_n n(\omega_n, T) \hat{\rho}_S^I(t) \otimes \gamma_n(t) \\
& = \hat{\rho}_S^I(t) \int_0^\infty n(\omega, T) D(\omega) |g(\omega)|^2 \left( \int_0^t e^{i(\Delta\omega - \omega)t'} dt' \right) d\omega \\
& \approx \hat{\rho}_S^I(t) \left[ \pi n(\Delta\omega, T) D(\Delta\omega) |g(\Delta\omega)|^2 \right. \\
& \quad \left. + iP \int_0^\infty \frac{n(\omega, T) D(\omega) |g(\omega)|^2}{\Delta\omega - \omega} d\omega \right]. \tag{54}
\end{aligned}$$

Here, we extend the upper limit of the time integration to infinity. The equation of motion for the dot system is finally reduced to

$$\begin{aligned} \dot{\rho}_S^I(t) = & iU(r)[\hat{A}^\dagger \hat{B}_2 + \hat{B}_2^\dagger \hat{A}, \hat{\rho}_S^I(t)] - n\gamma(\{\hat{C}\hat{C}^\dagger, \hat{\rho}_S^I(t)\} - 2\hat{C}^\dagger \hat{\rho}_S^I(t) \hat{C}) \\ & - (1+n)\gamma(\{\hat{C}^\dagger \hat{C}, \hat{\rho}_S^I(t)\} - 2\hat{C} \hat{\rho}_S^I(t) \hat{C}^\dagger), \end{aligned} \quad (55)$$

where  $n \equiv n(\Delta\omega, T)$  and  $\gamma \equiv \pi D(\Delta\omega)|g(\Delta\omega)|^2$ . The terms indicating the energy shift are neglected in (55) because the shift is usually small in the case of weak coupling between the quantum-dot system and phonon reservoir.

Let us consider one-exciton dynamics in the system, using three bases, as illustrated in Fig. 8. The equations of motion for the matrix elements are then read in the Schrödinger picture as

$$\dot{\rho}_{11}(t) = iU(r)[\rho_{12}(t) - \rho_{21}(t)], \quad (56)$$

$$\dot{\rho}_{12}(t) - \dot{\rho}_{21}(t) = 2iU(r)[\rho_{11}(t) - \rho_{22}(t)] - (1+n)\gamma[\rho_{12}(t) - \rho_{21}(t)], \quad (57)$$

$$\dot{\rho}_{22}(t) = -iU(r)[\rho_{12}(t) - \rho_{21}(t)] - 2(1+n)\gamma\rho_{22}(t) + 2n\gamma\rho_{33}(t), \quad (58)$$

$$\dot{\rho}_{33}(t) = 2(1+n)\gamma\rho_{22}(t) - 2n\gamma\rho_{33}(t), \quad (59)$$

where  $\rho_{mn}(t) \equiv \langle \Phi_m | \hat{\rho}_S(t) | \Phi_n \rangle$  is employed. When the temperature,  $T$ , equals zero ( $n = 0$ ), (56–59) can be solved analytically. The diagonal parts representing the population probability for each energy level in QD-A and QD-B, as well as the off-diagonal parts representing quantum coherence, are given as

$$\rho_{11}(t) = \frac{1}{Z^2} e^{-\gamma t} \left[ \frac{\gamma}{2} \sinh(Zt) + Z \cosh(Zt) \right]^2, \quad (60)$$

$$\rho_{22}(t) = \frac{U^2}{Z^2} e^{-\gamma t} \sinh^2(Zt), \quad (61)$$

$$\rho_{33}(t) = 1 - [\rho_{11}(t) + \rho_{22}(t)], \quad (62)$$

$$\rho_{12}(t) = -\rho_{21}(t) = i \frac{U}{Z^2} e^{-\gamma t} \sinh(Zt) \left[ \frac{\gamma}{2} \sinh(Zt) + Z \cosh(Zt) \right], \quad (63)$$

where  $Z \equiv \sqrt{(\gamma/2)^2 - U^2}$ , and initial conditions  $\rho_{11}(0) = 1$  and  $\rho_{12}(0) = \rho_{21}(0) = \rho_{22}(0) = \rho_{33}(0) = 0$  are used. We define the state-filling time  $\tau_S$  as  $\rho_{33}(\tau_S) = 1 - e^{-1}$ , which corresponds to the time for the excitation energy

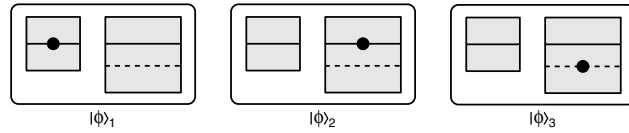


**Fig. 8.** Three bases of the single-exciton state in a two-quantum-dot system

Progress in Nano-Electro-Optics V  
Nanophotonic Fabrications, Devices, Systems, and  
Their Theoretical Bases

Ohtsu, M. (Ed.)

2006, XIV, 188 p., Hardcover

ISBN: 978-3-540-28665-3